



Sorption of trivalent lanthanides and actinides onto montmorillonite: Macroscopic, thermodynamic and structural evidence for ternary hydroxo and carbonato surface complexes on multiple sorption sites



M. Marques Fernandes^{a, *}, A.C. Scheinost^{b, c}, B. Baeyens^a

^a Paul Scherrer Institute, Laboratory for Waste Management, 5232 Villigen PSI, Switzerland

^b Helmholtz Zentrum Dresden Rossendorf e.V. (HZDR), Institute of Resource Ecology, 01314 Dresden, Germany

^c The Rossendorf Beamline at ESRF, 38043 Grenoble, France

ARTICLE INFO

Article history:

Received 22 January 2016

Received in revised form

5 April 2016

Accepted 17 April 2016

Available online 21 April 2016

Keywords:

Trivalent actinides

Clay minerals

Carbonate complexation

2SPNE SC/CE model

Strong and weak sites

TRLFS

EXAFS

ABSTRACT

The credibility of long-term safety assessments of radioactive waste repositories may be greatly enhanced by a molecular level understanding of the sorption processes onto individual minerals present in the near- and far-fields. In this study we couple macroscopic sorption experiments to surface complexation modelling and spectroscopic investigations, including extended X-ray absorption fine structure (EXAFS) and time-resolved laser fluorescence spectroscopies (TRLFS), to elucidate the uptake mechanism of trivalent lanthanides and actinides (Ln/An^{III}) by montmorillonite in the absence and presence of dissolved carbonate. Based on the experimental sorption isotherms for the carbonate-free system, the previously developed 2 site protolysis non electrostatic surface complexation and cation exchange (2SPNE SC/CE) model needed to be complemented with an additional surface complexation reaction onto weak sites. The fitting of sorption isotherms in the presence of carbonate required refinement of the previously published model by reducing the strong site capacity and by adding the formation of Ln/An^{III}-carbonato complexes both on strong and weak sites. EXAFS spectra of selected Am samples and TRLFS spectra of selected Cm samples corroborate the model assumptions by showing the existence of different surface complexation sites and evidencing the formation of Ln/An^{III} carbonate surface complexes. In the absence of carbonate and at low loadings, Ln/An^{III} form strong inner-sphere complexes through binding to three Al(O,OH)₆ octahedra, most likely by occupying vacant sites in the octahedral layers of montmorillonite, which are exposed on {010} and {110} edge faces. At higher loadings, Ln/An^{III} binds to only one Al octahedron, forming a weaker, edge-sharing surface complex. In the presence of carbonate, we identified a ternary mono- or dicarbonato Ln/An^{III} complex binding directly to one Al(O,OH)₆ octahedron, revealing that type-A ternary complexes form with the one or two carbonate groups pointing away from the surface into the solution phase. Within the spectroscopically observable concentration range these complexes could only be identified on the weak sites, in line with the small strong site capacity suggested by the refined sorption model. When the solubility of carbonates was exceeded, formation of an Am carbonate hydroxide could be identified. The excellent agreement between the thermodynamic model parameters obtained by fitting the macroscopic data, and the spectroscopically identified mechanisms, demonstrates the mature state of the 2SPNE SC/CE model for predicting and quantifying the retention of Ln/An^{III} elements by montmorillonite-rich clay rocks.

© 2016 Elsevier Ltd. All rights reserved.

1. Introduction

A major concern with high-level radioactive waste repositories in deep geologic formations is the potential release of radionuclides

(RNs) into the biosphere, which needs to be prevented for hundreds of thousands of years due to the long half-life of critical actinides and fission products. An important component of the safety case is the long-term prediction of RN binding to mineral components along the transport path. Sorption onto clay minerals as major constituents of engineered barriers and – in case of argillaceous host rocks – of the natural barriers, is a crucial process in the retardation chain, which needs to be understood on several length-

* Corresponding author.

E-mail address: maria.marques@psi.ch (M.M. Fernandes).

and time-scales in order to predict reliably the macroscopic RN migration through such clay-rich barriers.

In the near-field of deep-geologic high-level waste repositories, reducing conditions will prevail soon after closure, hence long-lived and radiotoxic actinides such as Ac, Pu, Am and Cm will be present in their trivalent oxidation state. In natural environments, the predominant aqueous reactions of trivalent actinides (An^{III}) and their chemical analogues, the trivalent lanthanides (Ln^{III}), are hydrolysis and complexation with dissolved inorganic ligands. Dissolved carbonate is of particular interest in this context due its ubiquity in surface and deep groundwaters, but also in the porewaters of host rocks and backfill materials (*i.e.* bentonite, cement). The in-situ porewater of Boom Clay for instance contains up to 10^{-2} M dissolved carbonate, the porewaters of Opalinus Clay, Callovian–Oxfordian clayrock and bentonite about 10^{-3} M (Baeyens et al., 2014; De Craen et al., 2004; Gaucher et al., 2006). Aqueous An^{III} carbonate complexes are very strong, and have been shown to reduce sorption at higher pH, and hence are expected to increase the migration rates of RNs (Guillaumont et al., 2003).

Surface complexation models based on macroscopic sorption experiments of metals on pure minerals are currently state-of-the-art tools to predict the sorption of RNs in clay rich environments under realistic geochemical conditions. Several studies have quantified and modelled the sorption of Ln/An^{III} on clay minerals in simple electrolyte, *i.e.* without organic and inorganic ligands (Bradbury and Baeyens, 2002, 2006; 2009a, b; Coppin et al., 2002; Gorgeon, 1994; Schnurr et al., 2015; Tertre et al., 2006). In the quasi mechanistic 2 site protolysis non electrostatic surface complexation and cation exchange (2SPNE SC/CE) model, sorption of Ln/An^{III} on montmorillonite and illite is predicted by taking into account three different site types, (1) cation exchange on planar sites, (2) surface complexation on strong sites ($\equiv S^{OH}$) with high affinity, but low capacity, and (3) surface complexation on weak sites ($\equiv S^{W1,2OH}$) with high capacity and low affinity (Bradbury and Baeyens, 2002). Such multi-site sorption behavior was also observed for other elements, *e.g.* divalent transition metals, UO_2^{2+} and NpO_2^+ on clay minerals (Bradbury and Baeyens, 2005, 2009a, b).

A quantitative description of the influence of dissolved carbonate on the sorption of Ln/An^{III} by clay minerals has been little examined until now. To the best of our knowledge, only two studies of Ln/An^{III} to montmorillonite and illite have focused on this issue (Marques Fernandes et al., 2008; Marques Fernandes et al., 2015). The observed decrease in sorption was less important than predicted by the model, in which Ln/An^{III} aqueous carbonate complexes were considered as non-sorbing. Only after complementing the model with two carbonate surface complexes on strong sites, $\equiv S^{OH}EuCO_3$ and $\equiv S^{OH}EuOHCO_3$, the data were reproduced. Since the study was conducted at trace concentration only, surface complexation reactions on weak sites were not determined.

Sorption models have a considerably higher reliability and credibility in their application of long-term predictions if they are supported by spectroscopically determined surface complexes. Time Resolved Laser Fluorescence Spectroscopy (TRLFS) is a very efficient speciation tool for Ln/An^{III} in aqueous solutions or at mineral-water interfaces and enabled the discrimination and quantification of Eu^{III} or Cm^{III} species sorbed by different clay minerals (Geckeis et al., 2013; Schnurr et al., 2015). For instance, the existence of Cm^{III} carbonate complexes at kaolinite and $\gamma-Al_2O_3$ surfaces could be proven by TRLFS (Marques Fernandes et al., 2010). However, TRLFS probes only the ligand field of susceptible metal centers, hence information on the short range structure is limited. Extended X-ray Absorption Fine Structure (EXAFS) spectroscopy is currently the most appropriate and most widely applied spectroscopic technique to probe the atomic-scale environment of metal ions (Brown and Sturchio, 2002). Its use allows identifying the

uptake mechanism of actinides and other metal ions including formation of outer- and inner-sphere complexes and the incorporation by the sorbing mineral itself or by surface precipitates (Denecke, 2006; Tan et al., 2010). In experiments containing dissolved carbonate, EXAFS evidenced the formation of U^{VI} -carbonate surface complexes on minerals such as hematite, montmorillonite, and ferrihydrite (Bargar et al., 1999, 2000; Catalano and Brown, 2005; Rossberg et al., 2009). The use of EXAFS together with calculations based on density functional theory (DFT) also enabled the structural visualization of different binding sites for Zn^{II} on montmorillonite, consistent with a multi-site sorption behavior and in particular with the strong-weak site concept of the 2SPNE SC/CE model (Churakov and Dähn, 2012; Dähn et al., 2011). The divalent Zn cation can adopt, due to its size and crystal field stabilization, either an octahedral or a tetrahedral coordination to oxygen ligands, and hence fits into the crystal lattice of montmorillonite. In contrast, the trivalent early actinides and early lanthanides have much larger ionic radii and are therefore typically nine-coordinated, adopting a tricapped prismatic coordination structure (Galbis et al., 2010; Kirsch et al., 2011; Persson et al., 2008). It seems therefore much less likely, that the observed strong-site sorption behavior of An/Ln^{III} is also based on their partial incorporation into the clay lattice.

In general, structural data of An/Ln^{III} complexes formed on minerals and particularly on clay minerals are very sparse. In an attempt to probe the structure of Am^{III} sorbed on smectite by EXAFS, only the first oxygen coordination shell could be identified (Stumpf et al., 2004). In three other studies, EXAFS was applied to elucidate the binding mechanism of Lu^{III} , Eu^{III} and Am^{III} sorbed to and co-precipitated with hectorite (Finck et al., 2012, 2015, 2009). For these three elements, EXAFS allowed to discriminate between surface complexes in case of sorption, and structural incorporation in case of co-precipitation. The sorption mechanism was consistent with the formation of inner-sphere surface complexes at the edges of hectorite platelets.

In the current study, the sorption of trivalent actinides and lanthanides at the montmorillonite surface under different experimental conditions is investigated. Firstly, we measured sorption isotherms across a large concentration range in the presence/absence of dissolved carbonate. Secondly, we refined the 2 SPNE SC/CE model based on these wet chemical data. Finally, we used TRLFS and EXAFS to identify the major surface complexes in the different systems, including postulated ternary surface complexes on strong and weak sites, and to unravel their local structure. The combination of complementary information based on wet chemistry, surface complexation modelling and spectroscopy allowed us to obtain a refined picture of the sorption processes from the atomic to the macroscopic scale.

2. Experimental

2.1. Materials

Supra-pure grade chemicals and ultra-pure deionized water ($18 M\Omega\text{ cm}^{-1}$) were used to prepare the solutions. A conditioned and purified Na-montmorillonite¹ suspension in 0.1 M $NaClO_4$ was used for the sorption experiments and the TRLFS and EXAFS samples. Details on the clay purification can be found elsewhere (Baeyens and Bradbury, 1995). Based on their very close thermodynamic properties, trivalent Eu, Cm and Am are often used as chemical analogues (Choppin, 1995). In this study we used Eu to

¹ Texas montmorillonite (STx-1) from the Clay Minerals Society Source Clay Repository.

measure the sorption isotherms. Because of its very sensitive fluorescence properties (higher molar absorptivity), Cm was used for the TRLFS measurements. Finally, Am was chosen for the EXAFS samples, since the Eu-L X-ray adsorption edges interfere with the Fe-K absorption edge originating from the structural Fe content of STx-1 (0.5 wt %). Carbonate free samples were prepared in a glove box under N₂-atmosphere (O₂ < 3 ppm) to avoid any carbonate contamination. Experiments in the presence of carbonate were carried out under atmospheric conditions in closed polycarbonate vessels.

2.2. Sorption isotherms

The sorption of Eu on homo-ionic Na-STx-1 was measured as a function of Eu concentration in 0.1 M NaClO₄ background electrolyte without carbonate at pH 8.0 and with carbonate at pH 9.2. The latter pH value was chosen because in a previous study we have observed that at pH 8 the effect of carbonate on the sorption is small compared to that at pH ~9 (Marques Fernandes et al., 2008). The samples were prepared in triplicates at a sorbent concentration (S) of 1 g L⁻¹ in 40 ml centrifuge tubes. Stable Eu solutions covering a concentration range of 10⁻⁹ to 10⁻⁴ M were prepared from Eu(NO₃)₃ in 0.1 M NaClO₄ and labelled with ¹⁵²Eu. The pH values of the carbonate free experiments were buffered with 2 · 10⁻³ M C₈H₁₇NO₃S (CHES) (BioChemika MicroSelect, Fluka). No pH buffer was used for the experiments in the presence of carbonate. To reproduce atmospheric pCO₂ conditions, the samples were pre-equilibrated with a mixture of NaHCO₃/Na₂CO₃ (7.4 · 10⁻³ M). The samples were shaken end-over-end for 7 days and then centrifuged at 105,000 g (max) for one hour using a Beckman Coulter Avanti™ J30I High-Performance centrifuge. The carbonate free samples were then returned to the glove box for sampling of the supernatant and pH measurements. The pH of each sample was measured immediately after radio-assay sampling using a Metrohm combination electrode calibrated with Merck buffers. The samples with carbonate had a mean pH value of 9.2 which corresponds to a pCO₂ of 10^{-3.7} bar, i.e. slightly lower than atmospheric pCO₂. The dissolved carbonate was not measured at the end of the experiments. In preliminary experiments, however, the evolution of the pH was followed between 2 and 60 days. The negligible variation of pH over this time period indicated that the carbonate concentration remained constant. Radiochemical assays of ¹⁵²Eu in the supernatants were performed with a Canberra Packard Cobra Quantum Gamma counter using standard labelled solutions for calibration.

The results of the batch sorption experiments are presented as the logarithm of the equilibrium concentration versus either the solid liquid distribution ratio, R_d,

$$R_d = \frac{(C_{init} - C_{eq}) \cdot V}{C_{eq} \cdot m} \quad (\text{L} \cdot \text{kg}^{-1})$$

or the quantity of metal sorbed, C_{sorb}

$$C_{sorb} = (C_{init} - C_{eq}) \cdot \frac{V}{m} \quad (\text{mol} \cdot \text{kg}^{-1})$$

with C_{init}, initial aqueous concentration of Ln/An^{III} (M), C_{eq}, equilibrium aqueous concentration of Ln/An^{III} (M), V, volume of liquid phase (L), m, mass of solid phase (kg).

2.3. TRLFS samples

The Cm stock solution with the isotopic composition ²⁴⁸Cm (89.7%), ²⁴⁶Cm (9.4%) and other Cm isotopes (<1%) was stored in concentrated HCl. Two Na-STx-1 samples with Cm in the absence

(Cm-Mont) and presence (Cm-MontC) of carbonate were prepared at pH 9 at fixed ionic strength (I = 0.1 M) and S ~ 2 g L⁻¹ in 20 mL polyethylene (HDPE) bottles (Zinsser Analytics) at 298 K. The total initial Cm concentration of each sample was 1.25 · 10⁻⁷ M. After adding Cm the pH value of the samples decreased to ~3 and was re-adjusted to ~6 by adding in small steps analytical-grade 0.1 M NaOH. This precaution was taken in order to prevent colloid generation and the precipitation of solid phases. Cm-MontC was in equilibrium with atmospheric pCO₂ at pH 9. In both systems no pH buffers were used to avoid a potential influence on the TRLFS spectra. Samples were stored for at least 2 days and periodically shaken. Preliminary kinetics experiments covering time periods between 2 and 60 days showed that equilibrium was already reached after 2 days. Speciation calculations showed that the Cm(CO₃)₂⁻ complex is the dominant aqueous complex under the experimental conditions (Guillaumont et al., 2003). From the literature it is known that aqueous Cm carbonate complexes have much higher fluorescence intensities (1.1 < FI < 3.9) than Cm inner-sphere complexes on clay minerals (0.005 < FI < 0.4) (Fanghänel et al., 1998; Rabung et al., 2005). In order to ensure that the measured fluorescence signal originated from the surface Cm complexes, TRLFS measurements were conducted on wet pastes obtained immediately after phase separation. The Cm loadings of both samples were ≤ 6 · 10⁻⁵ mol kg⁻¹ as determined from the ICP-MS measurements of the supernatants (detection limit ~ 5 · 10⁻¹⁰ M), more than one order of magnitude lower than the lowest loaded EXAFS samples (see Fig. 1). The TRLFS measurements were conducted as detailed in the Supplemental Information (S1).

2.4. EXAFS samples

A concentrated ²⁴³Am (t_{1/2} = 7370 y) solution was obtained by dissolving ²⁴³Am₂O₃ in 1 M HCl by microwave dissolution. The activity of the ²⁴³Am stock solution and the subsequently diluted solutions were determined by gamma spectrometry. Montmorillonite samples (S = 2 g L⁻¹) with increasing Am loadings were prepared in 200 ml polypropylene bottles in 0.1 M NaClO₄ at pH~8 in the absence of carbonate, and at pH~9.2 in the presence of dissolved carbonate by adding appropriate amounts of a 5 · 10⁻⁵ M ²⁴³Am stock solution (Table 1). The pH of the carbonate free samples was buffered by CHES (2 · 10⁻³ M), whereas no pH buffer was necessary for the samples in the presence of carbonate. The Am loadings on STx-1 were chosen based on sorption isotherms and modelling to probe preferentially surface complexes on the strong or on the weak sites (see Section 3.1). In addition, a sample with Am solely adsorbed on the planar sites by cation exchange (Am-MontCE) was prepared at pH 3.5 in 0.03 M NaClO₄. A summary of the Am samples and the experimental conditions is given in Table 1. After a reaction time of 14 days, 40 mL of each suspension was slowly filtrated through a 47 mm diameter filter with a 0.47 μm pore size (Millipore) to produce oriented self-supporting clay films in order to improve the sensitivity of the EXAFS measurements (Manceau et al., 1998). The filtrations were conducted in a closed vessel. Further, the filtration of the carbonate free sample was carried out under a continuous flow of N₂ to avoid contamination by atmospheric carbonate and was returned to the glove box for drying. Each dried clay film was cut into 8 pieces and stacked on a plexiglas sample holder for EXAFS measurements.

To determine the ²⁴³Am loading of each sample, 40 ml of each clay suspension was centrifuged at 105,000 g (max) for one hour and the supernatants were radio-assayed for ²⁴³Am using gamma spectrometry. The Am-L₃ edge EXAFS spectra were collected at the Rossendorf Beamline at ESRF in fluorescence mode at room temperature. Additional experimental details on the EXAFS data acquisition and analysis are given in the S1.

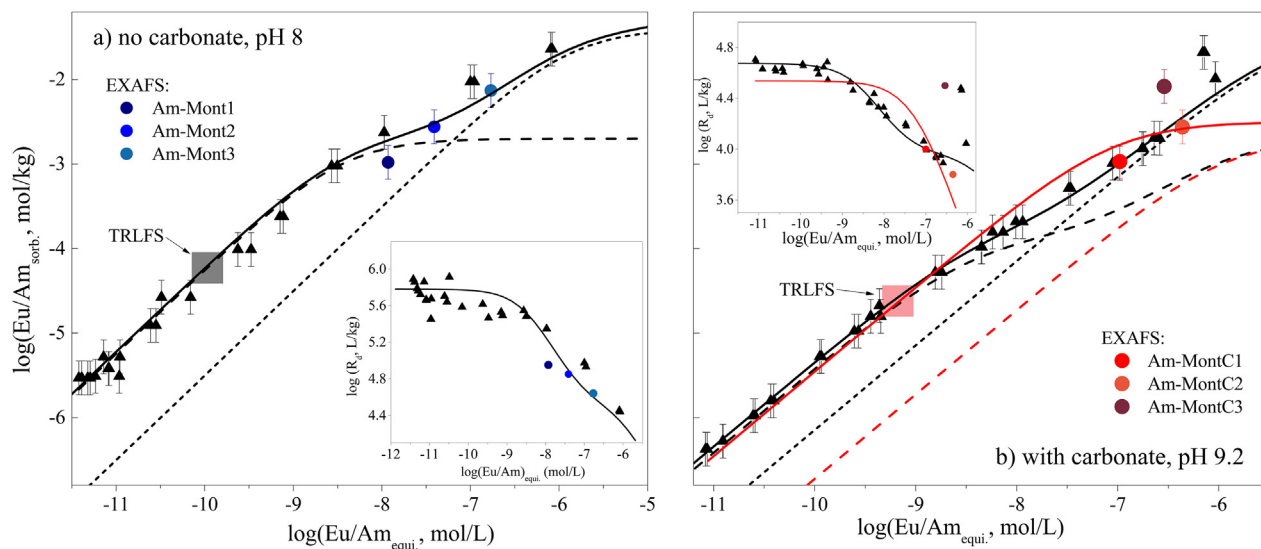


Fig. 1. Eu sorption isotherm on montmorillonite: a) in the absence of carbonate at pH 8 in 0.1 NaClO₄ and (b) with carbonate at pH 9.2 in 0.1 NaClO₄. The inserted figures depict the sorption plotted as $\log R_d$ vs. $\log C_{\text{eq}}$. Solid lines represent the calculated sorption isotherms of Am/Eu using the 2SPNE SC/CE model for montmorillonite. The contributions of the surface species on the strong edge sites ($\equiv\text{S}^{\text{S}}\text{COH}$) and the weak edge sites ($\equiv\text{S}^{\text{W}}\text{OH}$) to the overall metal sorption are illustrated by the black broken lines. In Fig. 1b, the red broken line is the calculated sorption isotherm when considering Am/Eu^{III}-carbonate complexes as non sorbing; the continuous red line is the modelled sorption with the earlier published surface complexation reactions and constants (Marques Fernandes et al., 2008). (For interpretation of the references to colour in this figure legend, the reader is referred to the web version of this article.)

The fit of the outer-sphere complex (Am-MontCE) and of the inner-sphere complexes (Am-Mont1 to -Mont3) was based on the structure of aluminocerite, where nine-coordinated Ce^{III} was replaced by Am (Nestola et al., 2009). The fit of the ternary, type-A, carbonate inner-sphere complexes (Am-MontC1 to MontC3) was based on the structure of Eu carbonate hydroxide (EuOHCO₃), which contains carbonate groups in both bidentate and monodentate coordination (C_{bid} , C_{mon}) (Michiba et al., 2011). Nine-fold coordinated Eu was replaced by Am, and an Am-Al path was created by replacing one of the C_{mon} by an Al atom. For the first two samples (Am-MontC1 and Am-MontC2), only C_{bid} was found to be relevant, while no indication for C_{mon} was given by the EXAFS shell fit. The fit of C_{bid} was complemented by the strong tri- and tetra-legged multiple scattering paths involving C_{bid} and its distal O (O_{dist}) following published approaches for U^{IV} carbonates, *i.e.* correlating the coordination number (CN), radial distance (R) and Debye-Waller factor (σ^2) of the Am- O_{dist} , Am- C_{bid} - O_{dist} and Am- C_{bid} - O_{dist} - C_{bid} paths (Hennig et al., 2010). The Fourier transform magnitude and imaginary part were fit in R -space in the range 0.9–3.3 Å for the samples with no carbonate, and between 0.9 and 4.3 Å for the samples with carbonate.

3. Results and discussion

3.1. Sorption isotherms

Fig. 1 shows the Eu sorption isotherms measured on conditioned

Na-STx-1 at pH ~8 in the absence of carbonate, and at pH ~9.2 in the presence of dissolved carbonate, along with $\log R_d$ plots as inserts. The experimental data are in line with previously published Eu isotherms and edges on SWy-1 montmorillonite (Bradbury and Baeyens, 2002; Marques Fernandes et al., 2008). The non-linearity of the log-log plots is characteristic of several different sorption site types. In the presence of carbonate the sorption of Eu is less pronounced and the isotherm is shifted by at least one order of magnitude to lower values, which complies with our previously published pH-edges at trace concentration (Marques Fernandes et al., 2008). At Eu equilibrium concentrations $>10^{-7}$ M, the uptake increases considerably, suggesting the precipitation of a solubility-limiting Eu carbonate phase (*e.g.* EuOHCO₃, NaEu(CO₃)₂) (Guillaumont et al., 2003). Note that the Am montmorillonite samples prepared for the EXAFS measurements follow well the respective Eu isotherms in the absence and presence of carbonate (coloured dots in Fig. 1a and b), confirming the chemical analogy of Am and Eu.

3.2. Sorption modelling

The sorption data was modelled with the 2SPNE SC/CE model for montmorillonite (Bradbury and Baeyens, 1997). A detailed description of the model and the modelling procedure is given in the S2.

In the absence of carbonate: The Eu sorption data in the absence of carbonate was modelled using the non-adjustable parameters

Table 1

EXAFS samples: $S = 2 \text{ g L}^{-1}$ in 0.1 M NaClO₄ or 0.03 M NaClO₄.

Sample	NaHCO ₃ /Na ₂ CO ₃ (M)	pH	²⁴³ Am _{eq} conc. (M)	²⁴³ Am sorbed (mol kg ⁻¹)	Log R _d (L kg ⁻¹)
Am-MontCE	—	3.5	$6.2 \cdot 10^{-7}$	$7.9 \cdot 10^{-3}$	4.1
Am-Mont1	—	8.0	$1.2 \cdot 10^{-8}$	$1.0 \cdot 10^{-3}$	4.9
Am-Mont2	—	8.0	$3.9 \cdot 10^{-8}$	$2.7 \cdot 10^{-3}$	4.8
Am-Mont3	—	8.0	$1.7 \cdot 10^{-7}$	$7.6 \cdot 10^{-3}$	4.6
Am-MontC1	$7.4 \cdot 10^{-3}$	9.2	$1.0 \cdot 10^{-7}$	$1.1 \cdot 10^{-3}$	4.0
Am-MontC2	$7.4 \cdot 10^{-3}$	9.2	$4.4 \cdot 10^{-7}$	$2.7 \cdot 10^{-3}$	3.8
Am-MontC3	$7.4 \cdot 10^{-3}$	9.2	$2.9 \cdot 10^{-7}$	$8.3 \cdot 10^{-3}$	4.5

given in Table S1 and the hydrolysis data from Table S2. The lower part of the isotherm ($[Eu]_{eq} \leq 10^{-8}$ M) could be reproduced with surface complexation reactions on the strong sites and the associated stability constants previously published (Marques Fernandes et al., 2008). To model the upper part, one additional reaction on weak sites ($\equiv S^{W1}OH$) was necessary. Fig. 1a shows the calculated Eu isotherm as solid line and the contribution of strong and weak sites as dashed and dotted lines, respectively. The surface complexation reactions and constants are summarized in Table S3. Based on the modelling results and the chemical analogy of Eu and Am, Am should form predominantly surface complexes on strong sites in Am-Mont1 (100%) and Am-Mont2 (74%), and on weak sites in Am-Mont3 (74%).

In the presence of carbonate: In our earlier study, an Eu sorption edge in the presence of carbonate was modelled by assuming the formation of two Eu-carbonate surface complexes ($\equiv S^S EuOHCO_3^-$ and $\equiv S^S EuCO_3$) on strong sites only (Table S4) (Marques Fernandes et al., 2008). Not accounting for such ternary complexes underestimated the Eu uptake significantly. Note that solely strong sites were considered, since the sorption edges were measured at trace Eu concentration ($< 10^{-8}$ M), where it had to be assumed that sorption is mainly taking place on these sites. This previously developed model seems to reproduce at a first glance the sorption isotherm satisfactorily (Fig. 1b, red line). The plot of $\log R_d$ vs. $\log [Eu]_{eq}$ shown as insert demonstrates, however, that the model slightly underestimates the sorption at low $[Eu]_{eq}$ and – more importantly – does not properly follow the shape of the isotherm *i.e.* the inflexion point corresponding to the decrease of R_d at $[Eu]_{eq} \sim 10^{-9}$ M. Increasing the values of the surface complexation constants ($\equiv S^S EuOHCO_3^-$ and $\equiv S^S EuCO_3$) improved the fit at low $[Eu]_{eq}$ but had no effect on the shape of the isotherm (data not shown). The linear plot of the experimental data as R_d vs. amount sorbed (Fig. S1) is again non-linear, suggesting sites with different affinities (Hinz, 2001; Kinniburgh, 1986). To reproduce the new experimental data (particularly the shape), the sorption model for the carbonate system was refined by reducing the capacity of the strong sites available for Eu-carbonate complexes ($\equiv S^{SC}OH$) to $0.13 \text{ mmol kg}^{-1}$ and taking into account the formation of ternary Eu-carbonate surface complexes on strong and weak sites ($\equiv S^{SC, W1} EuOHCO_3^-$ and $\equiv S^{SC, W1} EuCO_3$). Fig. 1b shows the resulting isotherm (black line) and the individual contributions of strong sites (black dashed line) and weak sites (black dotted line). The new sorption reactions and constants as well as modifications of non-adjustable parameters are summarized in Table S5. It should be noted that this model also reproduces well the pH dependent sorption data of the previous study (Fig. S2).

Based on our new modelling results, Am should occupy mainly the weak sites in Am-MontC1 and Am-MontC2. The enhanced uptake in Am-MontC3 also agrees with the isotherm data and reflects again the precipitation of a solubility-limiting Am carbonate phase. Nevertheless the (refined) fits reproduce the experimental data across a wide concentration range of more than 5 orders of magnitude well; this does not necessarily imply that the model is a unique solution, or in other words, that the postulated sorption processes are correct. We therefore employed TRLFS and EXAFS spectroscopy to study the structural environment of the different Ln/Am^{III} sorption complexes in order to verify the validity of our model assumptions.

3.3. TRLFS

The information provided by Cm^{III} TRLFS is twofold: (i) changes in the ligand field are detectable from spectral shifts of the ($^6D_{7/2} \rightarrow ^8S_{7/2}$) transition; the magnitude of the shift is correlated to the extent of covalent bonding to the ligands within the first

coordination sphere of the probed Cm ion, and (ii) the Cm fluorescence decay rate allows the hydration state of the given Cm species to be determined. If no other quench processes (*e.g.* metal to ligand transfer) are present in the vicinity of Cm, the rate of the radiationless de-excitation is directly proportional to the number of H₂O ligands in the inner coordination sphere of the Cm ion. Replacing these entities by other ligands through aqueous complexation reactions (hydrolysis, carbonate complexation etc.), sorption or incorporation on/in mineral phases, generally increases the fluorescence lifetime (Edelstein et al., 2006; Kimura and Choppin, 1994).

The emission spectra of the Cm/montmorillonite system in the absence (Cm-Mont) and presence of carbonate (Cm-MontC) obtained by exciting indirectly at $\lambda_{ex} = 396.6$ nm are shown in Fig. 2. In both cases the emission spectra are rather broad (full width at half maximum is ~ 11 nm for Cm-Mont and ~ 7 nm for Cm-MontC). This “inhomogeneous broadening” is typical for poorly ordered coordination environments (*e.g.* in glassy matrices, sorption complexes). In that case Cm ions occupy slightly different $^6D_{5/2}$ levels, which results in a continuous distribution of overlapping emission bands at different wavelengths.

In the absence of carbonate, the emission spectrum of Cm exhibits a peak maximum at ~ 602.4 nm, typical for inner-sphere sorption on clay minerals (Edelstein et al., 2006; Geckeis et al., 2013). In the presence of carbonate the maximum of the fluorescence emission band is shifted to ~ 604.6 nm, indicating a change in the first coordination sphere of Cm. The emission band maxima for Cm surface complexes published in the open literature are usually found at $\lambda_{max} \leq 607$ nm. For the carbonate free sample, the fluorescence lifetime decays mono-exponentially indicating that only one hydrated Cm species exists (Fig. 2, insert). The measured lifetime is about $\tau_{1a} = 117 \pm 5 \mu\text{s}$, which in a good agreement with the value of $\sim 110 \pm 5 \mu\text{s}$ for carbonate free Cm/clay suspensions (Edelstein et al., 2006; Geckeis et al., 2013). This lifetime correlates with the formation of a Cm inner sphere complex at the montmorillonite surface having ~ 5 H₂O molecules in the first hydration sphere. For the carbonate-containing system, the fluorescence lifetime shows a bi-exponential decay behaviour with lifetimes of $\tau_{2a} = 133 \pm 5 \mu\text{s}$ and $\tau_{3a} = 380 \pm 12 \mu\text{s}$ (Fig. 2 insert) suggesting the

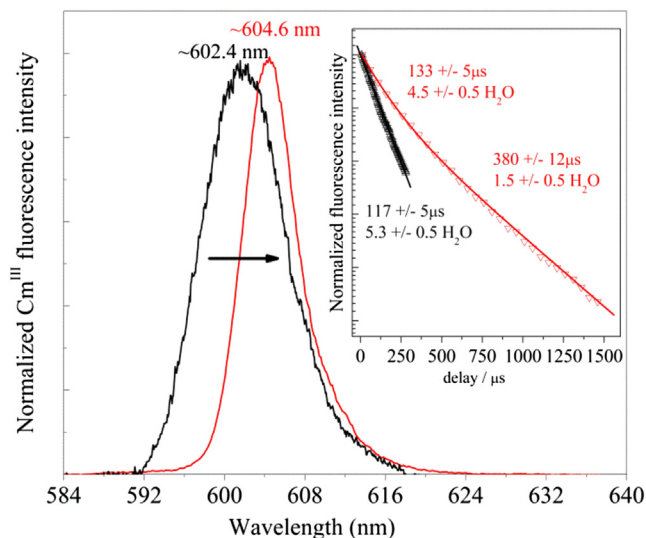


Fig. 2. Emission spectra of the $^6D_{7/2} \rightarrow ^8S_{7/2}$ transitions of Cm^{III} sorbed on montmorillonite in the absence (black line) and presence of carbonate (red line) and the corresponding fluorescence decay profiles (insert). (For interpretation of the references to colour in this figure legend, the reader is referred to the web version of this article.)

presence of (at least) two Cm species, one coordinated to an average of 4.5 H₂O and the other to an average of 1.5 H₂O molecules. The increase in the lifetimes compared to the carbonate free system reflects the formation of inner sphere complexes in which additional water molecules have been excluded and/or been replaced by CO₃²⁻ in the Cm coordination sphere. The change of the fluorescence features in the presence of dissolved carbonate *i.e.* the red-shift of the emission spectra and the increase of fluorescence lifetimes are in line with the results obtained on kaolinite and γ -Al₂O₃ (Marques Fernandes et al., 2010). The clear spectroscopic differences between the carbonate free and the carbonate containing system along with the thermodynamic prediction of Cm(CO₃)_n³⁻²ⁿ as predominant aquo complex under the given experimental conditions strongly suggests that the Cm^{III} species identified are Cm^{III} carbonate surface complexes.

3.4. EXAFS

Fig. 3 shows the Am-L_{III} EXAFS spectra of the montmorillonite samples as k³-weighted Fourier transform magnitude (FTM) and chi spectra (insert). The FTM represents the radial distribution function around the absorber atom Am, if one considers the phase shift ΔR of about 0.3–0.5 Å to the real distances R.

Cation exchange: The FTM of Am-MontCE shows only one significant peak at $R+\Delta R \approx 1.9$ Å, corresponding to nine oxygens from the hydration sphere of Am at a fitted distance of 2.47 Å (Table 2). The ninefold coordination is consistent with that of other solvated trivalent actinides up to Bk³⁺, Cf³⁺ being the first actinide showing the contraction to eightfold coordination (Galbis et al., 2010). It was therefore fixed during the fit, resulting in no significant reduction of the fit quality. The distance of 2.47 Å is in line with distances of 2.47–2.49 Å determined previously for the aqua ion and for outer-sphere complexes (cation exchange) on smectite and kaolinite (Allen et al., 2000; Stumpf et al., 2004). Note that the small side lobes on both sides of the main FTM peak do not arise from atomic interactions, but are truncation artifacts caused by the Fourier transformation of the finite, and rather short, chi function. Therefore, the EXAFS data of sample Am-MontCE shows as expected only the local coordination of the Am³⁺ aqua ion, confirming the cation exchange mechanism.

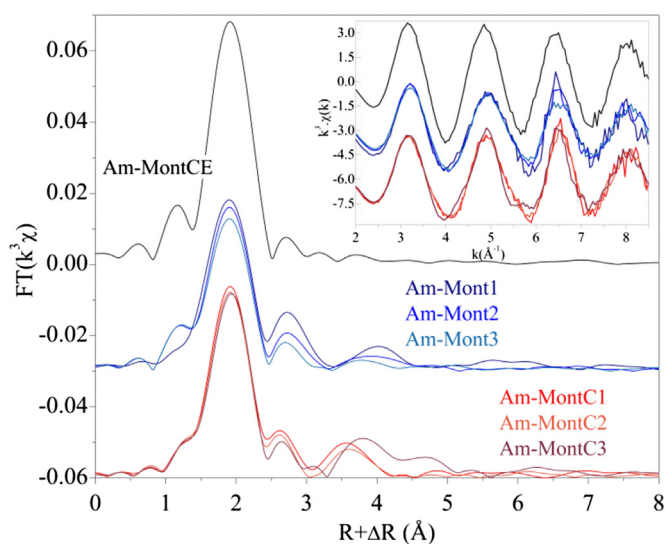


Fig. 3. Am-L_{III} EXAFS spectra of Am sorption samples on montmorillonite (see Table 1). The main figure shows the spectra as Fourier Transform Magnitude (FTM), the insert the corresponding k³-weighted EXAFS spectra.

In the absence of carbonate: For the (expected) inner-sphere complexes Am-Mont1 to Am-Mont3, the freely fitted first-shell CNs were smaller than 9, in line with previous EXAFS studies on Ln/An³⁺ inner-sphere complexes (Finck et al., 2012, 2015). However, the fitted Am-O distances of 2.46 Å are only 0.01 Å smaller than that of the aquo complex (Table 2), strongly suggesting that the coordination of the surface complexes remains also nine-fold, in line with the surface complex of another trivalent actinide, Pu, on magnetite (Kirsch et al., 2011). Therefore, we fixed the first-shell CN to nine for all samples, which resulted in stable fits with consistent fit values, and raised the fit error only insignificantly (Table 2). The coordination peak is followed by a much smaller peak at $R+\Delta R \approx 2.7$ Å, which decreases in height and distance from Am-Mont1 to Am-Mont3, and could be fitted with an Am-Al path. At a distance of 3.24 Å, there are about three Al for Am-Mont1 and about two Al atoms for Am-Mont2, while there is only one Al atom at a shorter distance of 3.20 Å for the sample with higher loading (Am-Mont3). The Am-Al distances and CNs obtained are well in line with formation of inner-sphere surface complexes between nine-fold coordinated Am and one, two and three Al(O,OH)₆ octahedra at the edges of montmorillonite sheets (Fig. 4). Note that possible Am-Si interactions at these positions could not be fitted, suggesting that they are either too far away, because the prevalent (010) and (110) faces are terminated rather by the octahedral than by the tetrahedral layers, or that they are not “visible” because of destructive interference between the Am-Si backscattering paths differing by about 0.2 Å in distance (Lee and Guggenheim, 1981). The absence of Am backscatterers in the FTM indicated that no Am^{III} solid phase such as Am(OH)₃ precipitated, in agreement with the sorption isotherm (Fig. 1a).

The coordination with one Al and the distance of 3.20 Å for the sample with highest loading (Am-Mont3) are well in line with the formation of bidentate, edge-sharing complexes towards the Al(O,OH)₆ octahedra protruding on the (010) faces of montmorillonite (Am¹ in Fig. 4). This complex coincides with Am sorption on weak sites predicted by the sorption model. In contrast, the sample with lowest loading, Am-Mont1, where modelling suggested Am surface complexation by strong sites, show a CN of three and longer distance for the Am-Al path. This EXAFS fit data can be consistently rationalized by Am residing in the near-surface vacant sites composed by a semi-circle of three Al octahedra (Am³ in Fig. 4). Note that these sites are on both the {010} and {110} faces of montmorillonite. At these sites, Am can establish at least four covalent bonds towards the three neighbouring Al octahedra, thereby providing a consistent structural explanation for the high thermodynamic stability of these surface complexes. For Am-Mont2, the CN of two could indicate binding of Am towards two Al octahedra as shown in Fig. 4 (Am²). A more plausible explanation for this difference is that this CN of 2.1 is a statistical mix of Am¹ and Am³, in line with the model prediction. While modelling predicts 26% on weak and 74% on strong sites, the EXAFS derived CN of 2.1 suggests a roughly 50/50 distribution between Am¹ and Am³. Considering the relatively high error of ± 0.5 for this CN, the amount of Am¹ may in fact vary between 20 and 80%, which includes the value predicted by the sorption model. Hence, also for sample Am-Mont2, both EXAFS and the model provide a consistent picture. In conclusion, the EXAFS results fully confirm the model prediction of strong and weak sites for Am at the montmorillonite edge faces, and provide a consistent structural model for these two surface complexes. Note that the structural basis for the strong site-weak site concept in sorption modelling has been provided earlier for the sorption of Zn onto montmorillonite (Dähn et al., 2011). While the structural incorporation of this divalent transition metal is very likely because of its close similarity in ionic radius and coordination geometry to Al and other cationic constituents of the octahedral

Table 2

Sample	1 st Coordination shell			Higher shells			ΔE_0 [eV]	χ^2_{res} %
	CN	R [Å]	σ^2 [Å ²]	CN	R [Å]	σ^2 [Å ²]		
Am-MontCE	9.0 ^f O	2.47	0.0074	-	-	-	7.2	5.9
Am-Mont1	9.0 ^f O	2.46	0.0126	3.0 Al	3.24	0.0077	8.0	5.1
Am-Mont2	9.0 ^f O	2.46	0.0138	2.1 Al	3.24	0.0095	8.3	5.1
Am-Mont3	9.0 ^f O	2.46	0.0150	1.0 Al	3.20	0.0054	7.7	6.1
Am-MontC1	9.0 ^f O	2.45	0.0118	1.3 Al	3.23	0.0030	7.6	6.4
				1.7 ^c C	2.97	0.0083		
				1.7 ^c O _{dist}	4.25 ^c	0.0030 ^c		
				3.4 ^{2c} C-O _{dist}	4.25 ^c	0.0030 ^c		
				1.7 ^c C-O _{dist} -C	4.25 ^c	0.0030 ^c		
Am-MontC2	9.0 ^f O	2.46	0.0125	0.9 Al	3.22	0.0030	7.7	7.4
				1.4 ^c C	2.94	0.0030		
				1.4 ^c O _{dist}	4.26 ^c	0.0030 ^c		
				2.8 ^{2c} C-O _{dist}	4.26 ^c	0.0030 ^c		
				1.4 ^c C-O _{dist} -C	4.26 ^c	0.0030 ^c		
Am-MontC3	9.0 ^f O	2.47	0.0127	1.0 ^f C	2.97	0.0030	7.5	6.3
				4.0 ^f C	3.47	0.0074		
				2.3 Am	4.00	0.0030		
				2.5 Am	4.60	0.0035		

CN: coordination number, error \pm 25%;

R: radial distance, error \pm 0.01 Å;

σ^2 : Debye-Waller factor, error \pm 0.0005 [Å²];

^f value fixed during the fit;

^c values coupled during the fit;

layers of montmorillonite, it is much more surprising that a similar mechanism holds also for much larger, nine-fold coordinated trivalent actinide, Am.

In the presence of carbonate: For the Am-MontC1 to Am-MontC2 samples, the first coordination peak is followed by a second peak at slightly shorter distance of 2.65 Å, and then by another peak at 3.6 to 3.8 Å raising significantly above the noise level. Since ternary carbonate complexes are predicted to form in these systems, we tested several different structural hypotheses, including formation of type-A (Am bridges between the clay surface and the carbonate ligand) and type-B (Am binds indirectly to the surface via an intermediate bridging carbonate ligand) ternary complexes with carbonate in either monodentate or bidentate coordination towards Am. For the two samples at lower Am-loading, Am-MontC1 and Am-MontC2, the only reliable fit was obtained with a type-A ternary complex, *i.e.* a surface-Am-carbonate arrangement, with carbonate in bidentate coordination towards Am (C_{bid}). This

structure gives rise to the relatively strong FTM peak at 3.6 Å because the distal oxygen (O_{dist}), as well as triple and four-legged multiple scattering paths involving C_{bid} and O_{dist}, have the same path lengths causing constructive interference. Only one distance and Debye-Waller factor needs to be fitted in this case, and the CNs are linked to that of C_{bid} (Hennig et al., 2010). The fit provided a good match of the experimental data and a Am-C distance of 2.94–2.97 Å consistent with bidentate coordination to the carbonate group. Furthermore, an Am-Al path with a distance of 3.22–3.23 Å was required, indicating as before a bidentate coordination towards Al(O,OH)₆ octahedra. The deduced local structure is fully consistent with formation of a type-A ternary carbonate complex, where Am³⁺ forms an edge-sharing complex with Al-octahedra of the montmorillonite edges, and is at the same time coordinated to 1–2 carbonate ligands (Am^{1c} in Fig. 4). Like for the carbonate-free samples, Am-Si paths could not be fitted, most likely due to a similar reason. The edge sharing coordination to one Al in analogy to the carbonate free system suggests that the Am-carbonato complexes are mainly located on the weak sites, thereby corroborating the refined sorption model.

The carbonate sample at the highest loading (Am-MontC3) could be fit with a structural model very close to Am carbonate hydroxide solid, based on the structure of Eu(CO₃)OH_(s) (Michiba et al., 2011). In this structure, the lanthanide/actinide cation center has one carbonate group in bidentate coordination and four carbonate groups in monodentate coordination. A good fit could be obtained by fixing the CNs to the crystallographic values. Adding the MS paths of C_{bid} did not improve the fit and was therefore omitted. The fitted shells (1 C at 2.97 Å, 4 C at 3.47 Å) are fairly well in line with the crystallographic structure (1 C at 2.95 Å, 4 C at 3.17 to 3.62 Å with an average distance of 3.42 Å). The FTM peak at 3.8 Å could be fitted with two different Am-Am shells, one at 4.00 Å and the other one at 4.60 Å. These distances agree well with the crystallographic data, with 6 Am-Am pairs between 3.90 and 4.19 Å giving an average of 4.06 Å, and one Am-Am pair at 4.63 Å. Since fixed CNs of 6 for the shorter Am and 1 for the longer one did not provide a satisfactory fit, the CNs were kept floating during the shell fit, resulting in CNs of about 2 for both shells. This significant deviation from the crystallographic values could be explained by

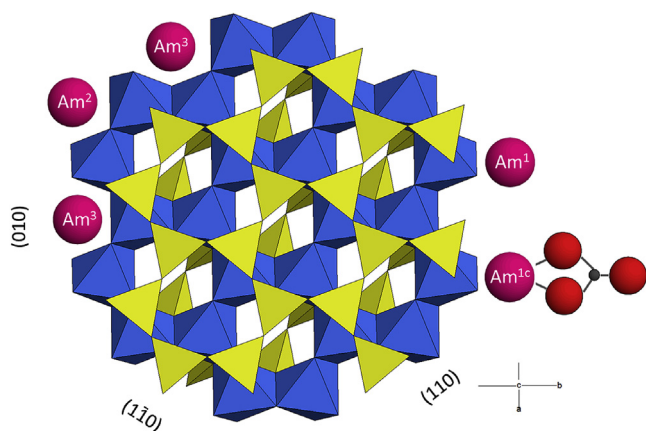


Fig. 4. Schematic sketch of possible Am binding sites on montmorillonite, with Am inner-sphere complexes involving one (Am¹), two (Am²) and three (Am³) aluminum neighbours. Am^{1c} is a type-A ternary carbonate complex. Al(O,OH)₆ octahedra are shown in blue, SiO₄ tetrahedra in yellow. (For interpretation of the references to colour in this figure legend, the reader is referred to the web version of this article.)

structural disorder, which is not supported by the small Debye-Waller factors. Hence a more likely explanation is a small particle size of the surface-induced precipitate as has been observed previously for instance for UO₂ or PuO₂ nanoparticles (Kirsch et al., 2011). Note that a previous attempt to fit the EXAFS spectrum of the corresponding Eu hydroxide carbonate allowed to extract only three shells in total (the coordination shell and two Eu-Eu shells at 3.81 and 4.20 Å) (Runde et al., 2000). In conclusion, the EXAFS spectrum of Am-MontC3 is indicative for the formation of an Am carbonate hydroxide precipitate. This is supported by the R_d value of this sample, which is significantly higher than for the lower loaded samples and strongly deviates from the sorption isotherm (Fig. 1b, Table 1).

4. Conclusion and implications

In the last decades, tremendous progress has been made in describing reactions at the solid-liquid interface by progressively moving from empirical approaches to surface complexation models based on thermodynamic equilibrium, the latter being the best current option to quantify sorption reactions at mineral surfaces, and ultimately to predict metal transport in subsurface environments. Sorption processes are strongly influenced by the geochemical conditions in the aquatic environment (e.g. pH, Eh, speciation of the sorbate, organic/inorganic ligands, competing ions) and by the properties of the mineral surface, e.g. surface groups and their charge. Hence, the development of robust and predictive thermodynamic sorption models, covering the widest range of relevant physico-chemical conditions in the porewater is crucial in order to assess the environmental risk. The quasi mechanistic 2 SPNE SC/CE model developed for illite and montmorillonite (few sorption site types, no multidentate binding modes) has shown to be capable of quantitatively reproducing sorption edges and isotherms for many metals (+I to +VI) under a wide variety of pH, ionic strength and metal concentration. Recently, the model has also been implemented to describe the sorption of Fe^{II} under different redox conditions (Soltermann et al., 2014). Applied in a bottom-up approach, it successfully blind-predicted sorption of many (radio-) contaminants in the clay rich rock formations, Opalinus Clay, Boda Clay, and bentonite in their complex porewater chemistries (Bradbury and Baeyens, 2011; Marques Fernandes et al., 2015).

Since there is no guarantee for the uniqueness of a solution extrapolated from a surface complexation model, investigating the main underlying physico-chemical processes at the molecular level by spectroscopic tools is a prerequisite to further refine and/or validate the sorption model. Here we demonstrate, using the sorption of trivalent lanthanides or actinides, to a typical clay mineral, montmorillonite, over a wide pH and concentration range and in the presence of dissolved carbonate, that the 2SPNE SC/CE model is capable to describe the main uptake processes. It does not only predict outer-sphere vs. inner-sphere sorption correctly, but also the formation of strong vs. weak inner-sphere complexes, as well as the formation of ternary Am-carbonate surface complexes on the weak sites, as we have verified by TRLFS and EXAFS spectroscopy.

Therefore, the good agreement between sorption modelling and spectroscopy (within the experimental, model and fitting uncertainties), is an encouraging step forward towards the reliability of safety assessment of radioactive waste repositories in argillaceous rocks. One important issue for which the model still needs to be further developed is its ability to account for competitive sorption. The structural identification of Am binding to specific aluminol sites at the edges of montmorillonite raises this issue, since from different EXAFS studies it is known that divalent metals

such as Zn, Fe, Ni also bind to these sites (Churakov and Dähn, 2012; Dähn et al., 2003; Soltermann et al., 2013).

Acknowledgement

We would like to thank Astrid Schaible and Vanessa Kalbermatter for technical assistance and Dr. Rainer Dähn for his support during the EXAFS measurements. The Institut für Nukleare Entsorgung (KIT, Germany) is acknowledged for the TRLFS pooled facility. The European Commission is acknowledged for financial support under the project JP 06-02 of the ACTINET Network of Excellence. Partial financial support was provided by the National Cooperative for the Disposal of Radioactive Waste, Nagra (Switzerland).

Appendix A. Supplementary data

Supplementary data related to this article can be found at <http://dx.doi.org/10.1016/j.watres.2016.04.046>.

References

- Allen, P.G., Bucher, J.J., Shuh, D.K., Edelstein, N.M., Craig, I., 2000. Coordination chemistry of trivalent lanthanide and actinide ions in dilute and concentrated chloride solutions. *Inorg. Chem.* 39 (3), 595–601.
- Baeyens, B., Bradbury, M.H., 1995. A Quantitative Mechanistic Description of Ni, Zn and Ca Sorption on Na-montmorillonite. Part I: Physico-chemical Characterization and Titration Measurements. PSI Bericht Nr 95-10, Villigen PSI, Switzerland.
- Baeyens, B., Thoenen, T., Bradbury, M.H., Marques Fernandes, M., 2014. Sorption Data Bases for Argillaceous Rocks and Bentonite for the Provisional Safety Analysis for SGT-E2. NTB 12-04, Nagra, Wettingen, Switzerland.
- Bargar, J.R., Reitmeyer, R., Lenhart, J.J., Davis, J.A., 2000. Characterization of U(VI)-carbonato ternary complexes on hematite: EXAFS and electrophoretic mobility measurements. *Geochim. Cosmochim. Acta* 64 (16), 2737–2749.
- Bargar, J.R., Reitmeyer, R., Davis, J.A., 1999. Spectroscopic confirmation of uranium(VI)-carbonato adsorption complexes on hematite. *Environ. Sci. Technol.* 33 (14), 2481–2484.
- Bradbury, M.H., Baeyens, B., 1997. A mechanistic description of Ni and Zn sorption on Na-montmorillonite. 2. Modelling. *J. Contam. Hydrol.* 27 (3–4), 223–248.
- Bradbury, M.H., Baeyens, B., 2002. Sorption of Eu on Na- and Ca-montmorillonites: experimental investigations and modelling with cation exchange and surface. *Geochim. Cosmochim. Acta* 66 (13), 2325–2334.
- Bradbury, M.H., Baeyens, B., 2005. Modelling the sorption of Mn(II), Co(II), Ni(II), Zn(II), Cd(II), Eu(III), Am(III), Sn(IV), Th(IV), Np(V) and U(VI) on montmorillonite: linear free energy relationships and estimates of surface binding constants for some selected heavy metals and actinides. *Geochim. Cosmochim. Acta* 69 (22), 875–892.
- Bradbury, M.H., Baeyens, B., 2006. Modelling sorption data for the actinides Am(III), Np(V) and Pa(V) on montmorillonite. *Radiochim. Acta* 94 (9–11), 619–625.
- Bradbury, M.H., Baeyens, B., 2009a. Sorption modelling on illite Part I: titration measurements and the sorption of Ni, Co, Eu and Sn. *Geochim. Cosmochim. Acta* 73 (4), 990–1003.
- Bradbury, M.H., Baeyens, B., 2009b. Sorption modelling on illite. Part II: actinide sorption and linear free energy relationships. *Geochim. Cosmochim. Acta* 73 (4), 1004–1013.
- Bradbury, M.H., Baeyens, B., 2011. Predictive sorption modelling of Ni(II), Co(II), Eu(III), Th(IV) and U(VI) on MX-80 bentonite and Opalinus Clay: a “bottom-up” approach. *Appl. Clay Sci.* 52 (1–2), 27–33.
- Brown, G.E., Sturchio, N.C., 2002. In: Fenter, P.A., Rivers, M.L., Sturchio, N.C., Sutton, S.R. (Eds.), *Applications of Synchrotron Radiation in Low-temperature Geochemistry and Environmental Science*. Mineralogical Society of America & Geochemical Society, Washington DC, 1–115.
- Catalano, J.G., Brown, G.E., 2005. Uranyl adsorption onto montmorillonite: evaluation of binding sites and carbonate complexation. *Geochim. Cosmochim. Acta* 69 (12), 2995–3005.
- Choppin, G.R., 1995. Comparative solution chemistry of the 4f and 5f elements. *J. Alloys Compd.* 223 (2), 174–179.
- Churakov, S.V., Dähn, R., 2012. Zinc adsorption on clays inferred from atomistic simulations and EXAFS spectroscopy. *Environ. Sci. Technol.* 46 (11), 5713–5719.
- Coppin, F., Berger, G., Bauer, A., Castet, S., Loubet, M., 2002. Sorption of lanthanides on smectite and kaolinite. *Chem. Geol.* 182 (1), 57–68.
- Dähn, R., Baeyens, B., Bradbury, M.H., 2011. Investigation of the different binding edge sites for Zn on montmorillonite using P-EXAFS – the strong/weak site concept in the 2SPNE SC/CE sorption model. *Geochim. Cosmochim. Acta* 75 (18), 5154–5168.
- Dähn, R., Scheidegger, A., Manceau, A., Schlegel, M., Baeyens, B., Bradbury, M.H., Chateigner, D., 2003. Structural evidence for the sorption of Ni(II) atoms on the

- edges of montmorillonite clay minerals: a polarized X-ray absorption fine structure study. *Geochim. Cosmochim. Acta* 67 (1), 1–15.
- De Craen, M., Wang, L., Van Geet, M., Moors, H., 2004. Geochemistry of Boom Clay pore water at the Mol site. SCK-CEN, Belgium. BLG-990, Mol.
- Denecke, M.A., 2006. Actinide speciation using x-ray absorption fine structure spectroscopy. *Coord. Chem. Rev.* 250 (7–8), 730–754.
- Edelstein, N.M., Klenze, R., Fanghanel, T., Hubert, S., 2006. Optical properties of Cm(III) in crystals and solutions and their application to Cm(III) speciation. *Coord. Chem. Rev.* 250 (7–8), 948–973.
- Fanghanel, T., Weger, H.T., Könnecke, T., Neck, V., Paviet-Hartmann, P., Steinle, E., Kim, J.L., 1998. Thermodynamics of Cm(III) in concentrated electrolyte solutions. Carbonate complexation at constant ionic strength (1M NaCl). *Radiochim. Acta* 82, 47–53.
- Finck, N., Bouby, M., Dardenne, K., Geckeis, H., 2012. Characterization of Eu(III) coprecipitated with and adsorbed on hectorite: from macroscopic crystallites to nanoparticles. *Mineral. Mag.* 76 (7), 2723–2740.
- Finck, N., Dardenne, K., Geckeis, H., 2015. Am(III) coprecipitation with and adsorption on the smectite hectorite. *Chem. Geol.* 409, 12–19.
- Finck, N., Schlegel, M.L., Bosbach, D., 2009. Sites of Lu(III) sorbed to and coprecipitated with hectorite. *Environ. Sci. Technol.* 43 (23), 8807–8812.
- Galbis, E., Hernández-Cobos, J., den Auwer, C., Le Naour, C., Guillaume, D., Simoni, E., Pappalardo, R.R., Sánchez Marcos, E., 2010. Solving the hydration structure of the heaviest actinide aqua ion known: the californium(III) case. *Angew. Chem.* 122 (22), 3899–3903.
- Gaucher, E.C., Blanc, P., Bardot, F., Braibant, G., Buschaert, S., Crouzet, C., Gautier, A., Girard, J.P., Jacquot, E., Lassin, A., Negrel, G., Tournassat, C., Vinsot, A., Altmann, S., 2006. Modelling the porewater chemistry of the callovian-oxfordian formation at a regional scale. *Cr. Geosci.* 338 (12–13), 917–930.
- Geckeis, H., Lützenkirchen, J., Polly, R., Rabung, T., Schmidt, M., 2013. Mineral–water interface reactions of actinides. *Chem. Rev.* 113 (2), 1016–1062.
- Gorgeon, L., 1994. Contribution à la modélisation physico-chimique de la rétention de radioéléments à vie longue par des matériaux argileux. PhD thesis (Paris VI).
- Guillaume, R., Fanghanel, T., Fuger, J., Grenthe, I., Neck, V., Palmer, D.A., Rand, M.H., 2003. Update on the Chemical Thermodynamics of Uranium, Neptunium, Plutonium, Americium and Technetium. Elsevier, Amsterdam.
- Hennig, C., Ikeda-Ohno, A., Emmerling, F., Kraus, W., Bernhard, G., 2010. Comparative investigation of the solution species $[\text{U}(\text{CO}_3)_5]^{6-}$ and the crystal structure of $\text{Na}_6[\text{U}(\text{CO}_3)_5] \cdot 12\text{H}_2\text{O}$. *J. Chem. Soc. Dalton Trans.* 39 (15), 3744–3750.
- Hinz, C., 2001. Description of sorption data with isotherm equations. *Geoderma* 99 (3–4), 225–243.
- Kimura, T., Choppin, G.R., 1994. Luminescence study on determination of the hydration number of Cm(III). *J. Alloys Compd.* 213, 313–317.
- Kinniburgh, D.G., 1986. General purpose adsorption isotherms. *Environ. Sci. Technol.* 20 (9), 895–904.
- Kirsch, R., Fellhauer, D., Altmair, M., Neck, V., Rossberg, A., Fanghanel, T., Charlet, L., Scheinost, A.C., 2011. Oxidation state and local structure of plutonium reacted with magnetite, mackinawite, and chukanovite. *Environ. Sci. Technol.* 45 (17), 7267–7274.
- Lee, J.H., Guggenheim, S., 1981. Single crystal X-ray refinement of pyrophyllite-1Tc. *Am. Mineral.* 66 (3–4), 350–357.
- Manceau, A., Chateigner, D., Gates, W.P., 1998. Polarized EXAFS, distance–valence least-squares modeling (DVLS), and quantitative texture analysis approaches to the structural refinement of Garfield nontronite. *Phys. Chem. Min.* 25 (5), 347–365.
- Marques Fernandes, M., Baeyens, B., Bradbury, M.H., 2008. The influence of carbonate complexation on lanthanide/actinide sorption on montmorillonite. *Radiochim. Acta* 96, 691–698.
- Marques Fernandes, M., Stumpf, T., Baeyens, B., Walther, C., Bradbury, M.H., 2010. Spectroscopic identification of ternary Cm–Carbonate surface complexes. *Environ. Sci. Technol.* 44 (3), 921–927.
- Marques Fernandes, M., Ver, N., Baeyens, B., 2015. Predicting the uptake of Cs, Co, Ni, Eu, Th and U on argillaceous rocks using sorption models for illite. *Appl. Geochem.* 59, 189–199.
- Michiba, K., Tahara, T., Nakai, I., Miyawaki, R., Matsubara, S., 2011. Crystal structure of hexagonal $\text{RE}(\text{CO}_3)\text{OH}$. *Z. Krist.* 226 (6), 518–530.
- Nestola, F., Guastoni, A., Cámara, F., Secco, L., Dal Negro, A., Pedron, D., Beran, A., 2009. Aluminocerite-Ce: a new species from Baveno, Italy: description and crystal-structure determination. *Am. Mineral.* 94 (4), 487–493.
- Persson, I., D'Angelo, P., De Panfilis, S., Sandström, M., Eriksson, L., 2008. Hydration of lanthanoid(III) ions in aqueous solution and crystalline hydrates studied by EXAFS spectroscopy and crystallography: the myth of the “Gadolinium Break”. *Chem. Eur. J.* 14 (10), 3056–3066.
- Rabung, T., Pierret, M.C., Bauer, A., Geckeis, H., Bradbury, M.H., Baeyens, B., 2005. Sorption of Eu(III)/Cm(III) on Ca-montmorillonite and Na-illite. Part 1: batch sorption and time-resolved laser fluorescence spectroscopy experiments. *Geochim. Cosmochim. Acta* 69 (23), 5393–5402.
- Rossberg, A., Ulrich, K.-U., Weiss, S., Tsushima, S., Hiemstra, T., Scheinost, A.C., 2009. Identification of uranyl surface complexes on ferrihydrite: advanced EXAFS data analysis and CD-MUSIC modeling. *Environ. Sci. Technol.* 43 (5), 1400–1406.
- Runde, W., Van Pelt, C., Allen, P.G., 2000. Spectroscopic characterization of trivalent f-element (Eu, Am) solid carbonates. *J. Alloys Compd.* 303, 182–190.
- Schnurr, A., Marsac, R., Rabung, T., Lützenkirchen, J., Geckeis, H., 2015. Sorption of Cm(III) and Eu(III) onto clay minerals under saline conditions: batch adsorption, laser-fluorescence spectroscopy and modeling. *Geochim. Cosmochim. Acta* 151, 192–202.
- Soltermann, D., Baeyens, B., Bradbury, M.H., Marques Fernandes, M., 2014. Fe(II) uptake on natural montmorillonites. II. Surface complexation modeling. *Environ. Sci. Technol.* 48 (15), 8698–8705.
- Soltermann, D., Marques Fernandes, M., Baeyens, B., Dahn, R., Mieke-Brendle, J., Wehrli, B., Bradbury, M.H., 2013. Fe(II) sorption on a synthetic montmorillonite. A combined macroscopic and spectroscopic study. *Environ. Sci. Technol.* 47 (13), 6978–6986.
- Stumpf, T., Hennig, C., Bauer, A., Denecke, M.A., Fanghanel, T., 2004. An EXAFS and TRLS study of the sorption of trivalent actinides onto smectite and kaolinite. *Radiochim. Acta* 92 (3), 133–138.
- Tan, X., Fang, M., Wang, X., 2010. Sorption speciation of lanthanides/actinides on minerals by TRLS, EXAFS and DFT studies: a review. *Molecules* 15 (11), 8431–8468.
- Tertre, E., Berger, G., Simoni, E., Castet, S., Giffaut, E., Loubet, M., Catalette, H., 2006. Europium retention onto clay minerals from 25 to 150 degrees C: experimental measurements, spectroscopic features and sorption modelling. *Geochim. Cosmochim. Acta* 70 (18), 4563–4578.